SSRG International Journal of Electrical and Electronics Engineering
ISSN: 2348-8379/ https://doi.org/10.14445/23488379/IJEEE-V11I10P119

Volume 11 Issue 10, 186-196, October 2024

Original Article

Multifunctional EV Charger with Bidirectional SEPIC Converter for Low Current Ripple in PV Source Supported Grid System

P. Vinay Kumar[1], P. Venkata Prasad[2], E. Vidhya Sagar[3]

[1,3]*Department of Electrical Engineering, University College of Engineering (A), Osmania University, Hyderabad, Telangana, India.*
[2]*Department of Electrical and Electronics Engineering Department, CBIT, Hyderabad, Telangana, India.*

[1]*Corresponding Author : vinayperumandla@gmail.com*

Received: 13 August 2024 Revised: 11 September 2024 Accepted: 12 October 2024 Published: 30 October 2024

Abstract *- A single-phase grid system with a PV source interconnected for renewable power sharing charging an EV battery is a complex design. At the DC link, the PV source and EV charger need to be connected for power exchange as per availability. The local residential load from the EV battery needs to be supported during grid islanding conditions. A multifunctional EV charger with a BD-SEPIC converter is proposed in this paper to achieve this. The BD-SEPIC converter can charge and discharge the EV battery per the system's requirements. The PV source is connected to the BD-SEPIC converter's input for power sharing to the grid or the EV battery. A single-phase voltage source full bridge converter connects the common DC link and the single-phase grid. The full bridge converter exchanges power between the grid, PV, and EV chargers based on grid availability. The full bridge converter is controlled by a central VSC control with a SOGI-FLL-DRC filter and SMC voltage regulator. The BD-SEPIC converter is controlled by V2G/G2V control. The power exchange between the modules is controlled as per the operation of the VSC and BD-SEPIC converter. An analysis of the proposed multi-module system with different operating conditions is carried out using the MATLAB Simulink software tool.*

Keywords *- Photo Voltaic (PV), Electric Vehicle (EV), Bidirectional SEPIC (BD-SEPIC), Voltage Source Converter (VSC), Second Order Generalized Integrator – Frequency locked Loop – DC (SOGI-FLL-DRC) offset rejection control, Sliding Mode Control (SMC), Vehicle to Grid/Grid to Vehicle (V2G/G2V), MATLAB Simulink.*

1. Introduction

Integrating PV systems with electric vehicle EV charging is an innovative approach that enhances energy sustainability and efficiency in urban and residential environments. This integration typically happens within the framework of a single-phase grid connection, which is commonly used in households and smaller commercial settings. Electric vehicles are gaining popularity due to their environmental benefits and advancements in battery technology. Charging these vehicles usually involves converting AC electricity from the grid into DC power suitable for EV batteries. This process can be optimized by leveraging the existing infrastructure of grid-connected PV systems [2].

PV systems generate clean electricity directly from sunlight, reducing fossil fuel dependency for transportation and electricity. By using solar energy for EV charging, households can cut their electricity bills and decrease the overall cost of vehicle ownership. Combining PV and EV charging reduces greenhouse gas emissions, helping to create a greener and more sustainable energy ecosystem. During peak sunlight hours, any excess solar power can be fed back into the grid, which helps to stabilize the grid and optimize energy distribution [3].

The PV system inverter must be correctly sized to handle household electricity needs and the additional load from EV charging. Using smart charging solutions allows for efficient use of solar energy by scheduling EV charging during peak sunlight hours. Integrating single-phase grid-connected PV systems with electric vehicle charging offers a promising way to enhance energy sustainability at the household level [4]. As technology advances and costs decrease, this synergy will likely become more accessible and widespread, contributing significantly to reducing carbon footprints and promoting the adoption of renewable energy [5].

In this paper, a single-phase system with a PV source and EV charging circuit is designed with grid interconnection. The PV source includes PV panels connected to a boost converter

operated by P&O MPPT for maximum power extraction [6]. The EV charging circuit comprises a BD-SEPIC converter, which charges and discharges the EV battery as per the switching of the MOSFETs [7].

A single-phase full bridge VSC is connected between the grid and the common DC link where the PV source and EV charging circuit are connected. The powers between these modules are exchanged by a central control that controls the VSC. Figure 1 represents the structure of the single-phase grid, PV source and EV charging module with BD-SEPIC and VSC circuits [6, 7].

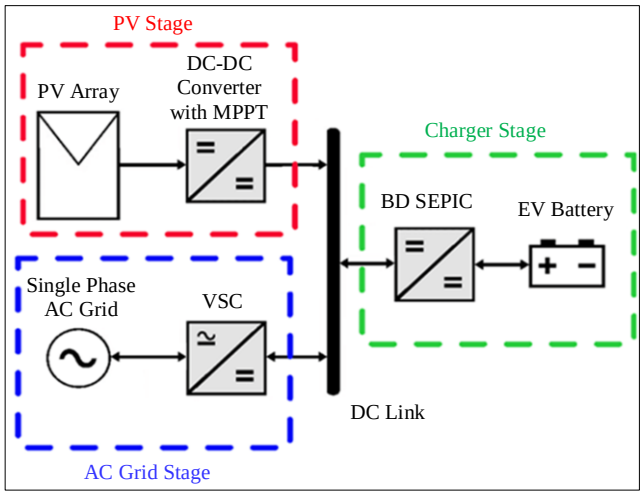

Fig. 1 Structure of proposed single-phase multifunctional EV charger

As observed in Figure 1, the PV stage only delivers power to the DC link, which is either shared with the grid or EV charging module. The AC grid stage can deliver or receive power from the PV stage or Charger stage through the VSC. The VSC controller controls the exchange of power between these modules, which receives feedback signals from the PV and Charger stages. The BD-SEPIC converter is controlled by an individual controller operating as per the system's requirements, either in V2G/or G2V modes [6].

This paper is arranged with an introduction to the proposed structure of the proposed single-phase multifunctional EV charger with PV source and grid connection in section 1. The following section 2 has the PV source and grid-connected VSC configuration, including the circuit structure and control design of the PV and AC grid stages. In section 3, the design of the BD-SEPIC converter is included with the circuit structure and V2G/G2V control design. The simulation analysis of the combined proposed system is analyzed in section 4, with a brief discussion of the results and graphs of each stage of the system. The conclusion to the paper is included in final section 5, validating the system's performance with the achieved simulation results, followed by references cited in the paper.

2. PV-Supported Grid System Configuration

Solar panels, also known as Photovoltaic (PV) panels, play a critical role in the shift towards renewable energy sources. They generate electricity without emitting greenhouse gases, significantly reducing the carbon footprint compared to fossil fuel-based power plants. Reducing reliance on fossil fuels helps alleviate climate change and its associated impacts, such as extreme weather events and rising sea levels. Solar energy production does not involve burning fuels, which means it does not release air pollutants like sulfur dioxide, nitrogen oxides, and particulate matter [8]. Additionally, it avoids water pollution from fossil fuel extraction and processing. Once installed, solar panels provide a source of free energy, significantly reducing electricity bills for homeowners and businesses alike. By generating electricity locally, solar panels decrease dependence on imported fuels, enhancing energy security and stability.

Solar panels can provide electricity in remote or underserved areas where it is impractical or too expensive to extend the grid [9]. This helps improve the quality of life and enables economic development in these areas. Solar installations can also be used as educational tools to raise awareness about renewable energy and encourage sustainable practices. Solar energy supports sustainable development by providing a reliable, long-term energy solution that meets present needs without compromising the ability of future generations to meet their own needs.

Installation of PV panels in residential buildings or commercial areas is very viable as the rooftops of these buildings can be filled with an array of panels. The array of panels generates accumulated solar power, which can either be consumed by local loads or injected into the grid. The solar power generated in residential applications is shared with a single-phase system [10]. The PV panels can be directly connected to a single-phase VSC or connected with a boost converter between the VSC and PV panels for maximum power extraction. There is an advantage of stabilizing and boosting the voltage with the boost converter connected to the VSC. Figure 2 represents the circuit structure of the proposed single-phase grid-connected PV panels.

The boost converter switch (Sb) is controlled by MPPT with a P&O (Perturb and Observe) algorithm that considers signals from PV array voltage (Vpv) and current (Ipv). At the boost converter's output, a single-phase full bridge VSC with four switches (S1-S4) is connected. This VSC is controlled by a power management controller with feedback from load current (iload), grid voltage (Vs) and DC link voltage (Vdc) [11]. The VSC need to operate in inverter or rectifier mode depending on the availability of PV power, load demand and grid availability. The pulses to the VSC are generated by the reference signal created by the power management controller. The complete structure of the power management controller is presented in Figure 3.

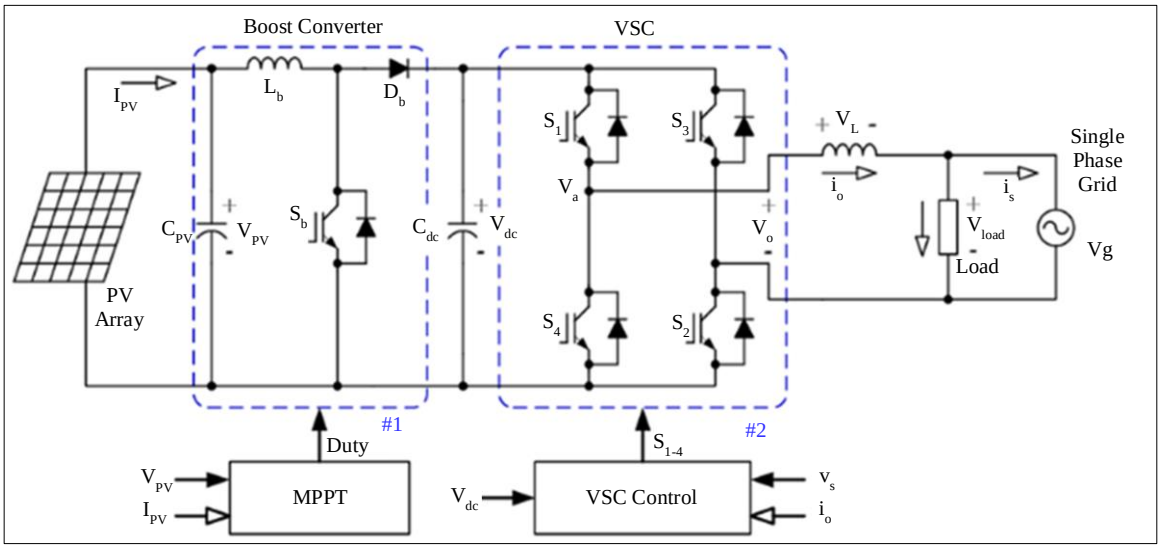

Fig. 2 Single-phase grid-connected PV array

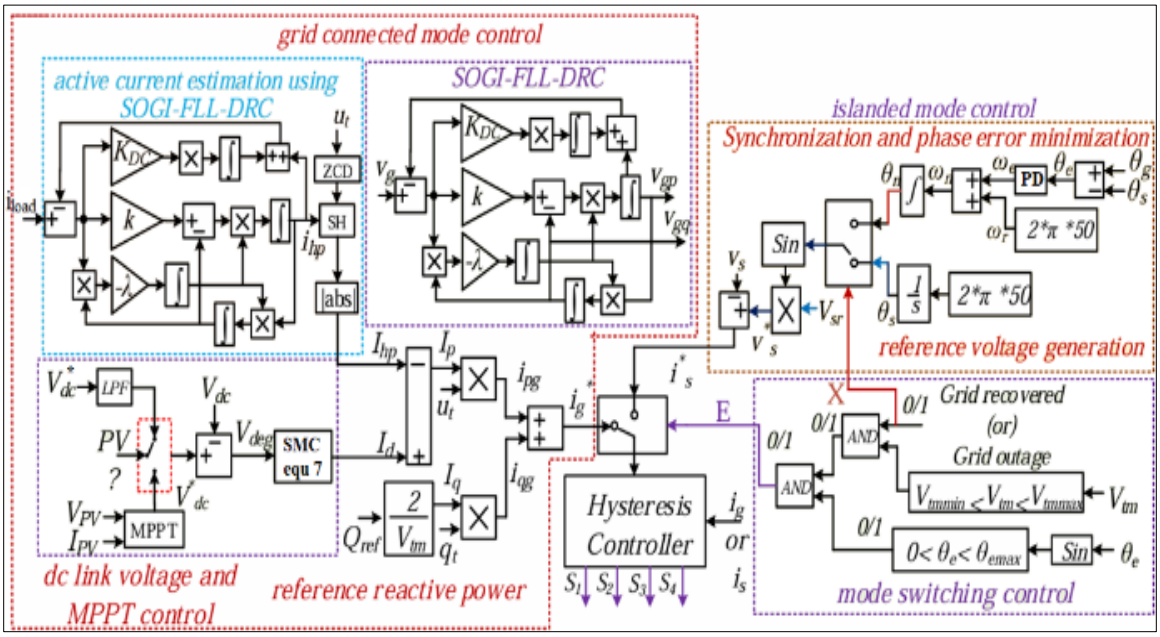

Fig. 3 Power management controller for VSC

As per Figure 3, it is determined that the VSC controller has two modes of control. The 'grid-connected mode control' is selected when the grid is available, and the 'islanding mode control' is selected when the grid is disconnected or unavailable [12]. This switching between the modes is controlled by 'mode switching control', which detects the grid availability. Reference current signals (i_s^* or i_g^*) are generated by these control modules with respect to the grid availability [13]. The current reference signals are given as follows:

$$i_g^* = i_{pg} + i_{qg} \quad (1)$$

$$i_s^* = V_s^* - V_s \quad (2)$$

Here, i_{pg} i_{qg} are active and reactive reference grid current components. V_s^* V_s are the reference and measured VSC voltage on the AC side. i_{pg} i_{qg} current components are calculated as:

$$i_{pg} = I_p u_t$$

$$i_{qg} = I_q q_t \quad (3)$$

In the given expression u_t q_t are the active and reactive power voltage vector templates generated by SOGI-FLL-DRC module active and reactive voltages $v_{gp} v_{gq}$ expressed as:

$$u_t = \frac{v_{gp}}{V_{tm}}$$

$$q_t = \frac{v_{gq}}{V_{tm}} \quad (4)$$

Here, V_{tm} is the root mean square of the v_{gp} v_{gq} values are given as:

$$V_{tm} = \sqrt{v_{gp}^2 + v_{gq}^2} \quad (5)$$

The i_p, i_q are the active and reactive calculated current magnitudes as per the load current (i_{load}), error voltage (V_{deg}), and reference reactive power (Q_{ref}) expressed as:

$$I_p = I_d - I_{hp}$$

$$I_q = Q_{ref}\frac{2}{V_{tm}} \quad (6)$$

I_{hp} is the active current estimation of load current (i_{load}) generated by the SOGI-FLL-DRC module. The direct axis current (I_d) is generated by the Sliding Mode Controller (SMC) expressed as [14],

$$I_d = C_{dc}V_{dc}\left[\left(\frac{1}{R_L C_{dc}} - \frac{1}{\gamma}\right)V_{dc} + \frac{1}{\gamma}V_{dc}^* - (\sigma + \delta)sing(S)\right] \quad (7)$$

In the given expression C_{dc} is the DC link capacitor, R_L is load resistance, V_{dc}^* reference DC link voltage, the constant values are given in configuration Table 1. The sliding variable (S) is determined as:

$$S = \gamma(V_{dc}^* - V_{dc}) + \int(V_{dc}^* - V_{dc})dt \quad (8)$$

The V_{dc}^* is selected as per the PV panel availability. If the PV module is connected and generates power, the V_{dc}^* is generated by the MPPT algorithm, or else the value is manually given by the user. In islanding mode V_s^* is generated from the fundamental angular frequency and error phase angle expressed as:

$$V_s^* = m\,Sin\,(\theta_s) \quad (9)$$

As per this value generated by the expression, the VSC switches are controlled by hysteresis current loop controller comparison of reference currents (i_s^* or i_g^*) to measured inverter or grid currents (i_s or i_g).

3. BD-SEPIC Converter Design

Designing and implementing a conventional bidirectional converter can be challenging due to the requirement for multiple switching devices, control circuits, and protection mechanisms. The complexity of the design and the need for high-quality components can increase the overall cost of the converter. Frequent switching of the power devices in the converter can lead to significant switching losses, especially at high frequencies. Resistance in the components and interconnections can result in conduction losses, decreasing the overall efficiency of the converter [15].

High-frequency switching in bidirectional converters can produce significant electromagnetic interference, impacting nearby electronic equipment and necessitating additional filtering. The losses in the converter generate heat, which must be effectively dissipated to prevent overheating and ensure reliable operation. This requirement entails robust thermal management solutions, which can increase the system's size, weight, and cost.

The switching operation can introduce harmonic distortion to the power system, which can impact the performance of other equipment [16]. This may necessitate additional filtering solutions. Integrating converters with renewable energy sources such as solar or wind can make it challenging to control and stabilize the bidirectional converter due to the intermittent nature of these sources. This requires advanced control strategies to manage fluctuations [17]. The ripple content in the voltage and currents in the DC sources increases the storage elements and load to a very high extent.

To solve these issues, the conventional DC/DC bidirectional converter is replaced with a BD-SEPIC converter with two MOSFET switches [18]. A bidirectional SEPIC converter can reverse the direction of power flow, allowing it to function as both a buck and boost converter. This feature is particularly useful for applications that require power to be transferred to and from an energy source, such as charging and discharging a battery. The SEPIC converter configuration provides a non-inverted output, meaning the output voltage polarity is the same as the input voltage.

This characteristic simplifies circuit design, especially when using components that are sensitive to polarity. Bidirectional SEPIC converters can efficiently manage a wide range of input and output voltages, making them suitable for systems with varying voltage requirements or when interfacing with different types of power sources and loads. Compared to other converters, SEPIC converters generally experience lower component stress, particularly on switches and inductors. This contributes to improved reliability and can extend the lifespan of the components, reducing the need for replacements and maintenance.

This converter is updated to the multifunctional EV charger capable of charging and discharging the EV battery as per the requirement. The change in duty ratio of these MOSFETs will change the operating direction and mode of the BD-SEPIC converter. The updated circuit structure to the PV array connected single phase grid system with BD-SEPIC multifunctional charger is presented in Figure 4.

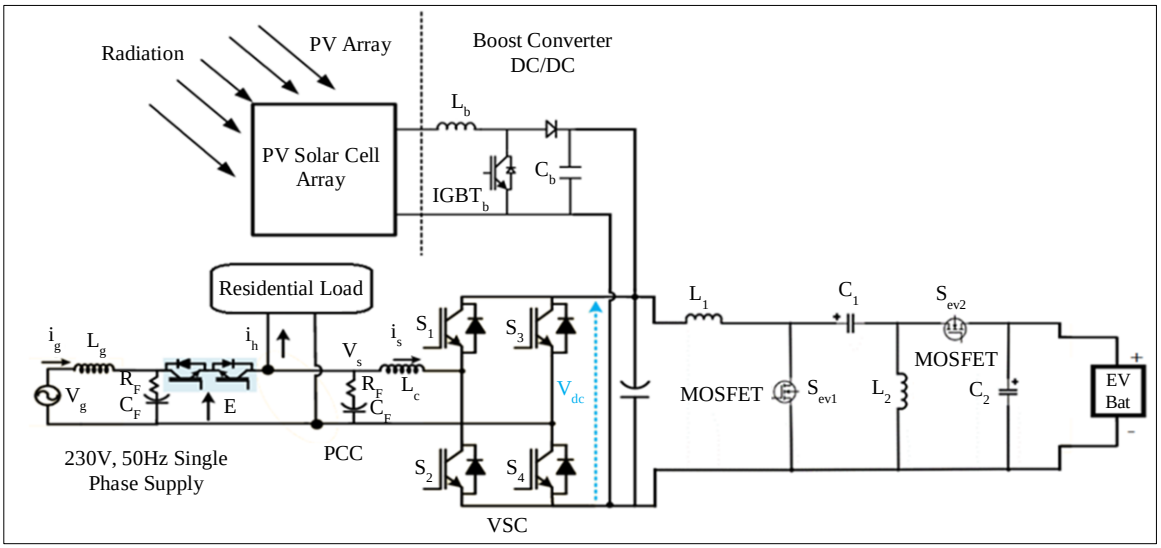

Fig. 4 Circuit structure with BD-SEPIC converter interconnected PV-grid system

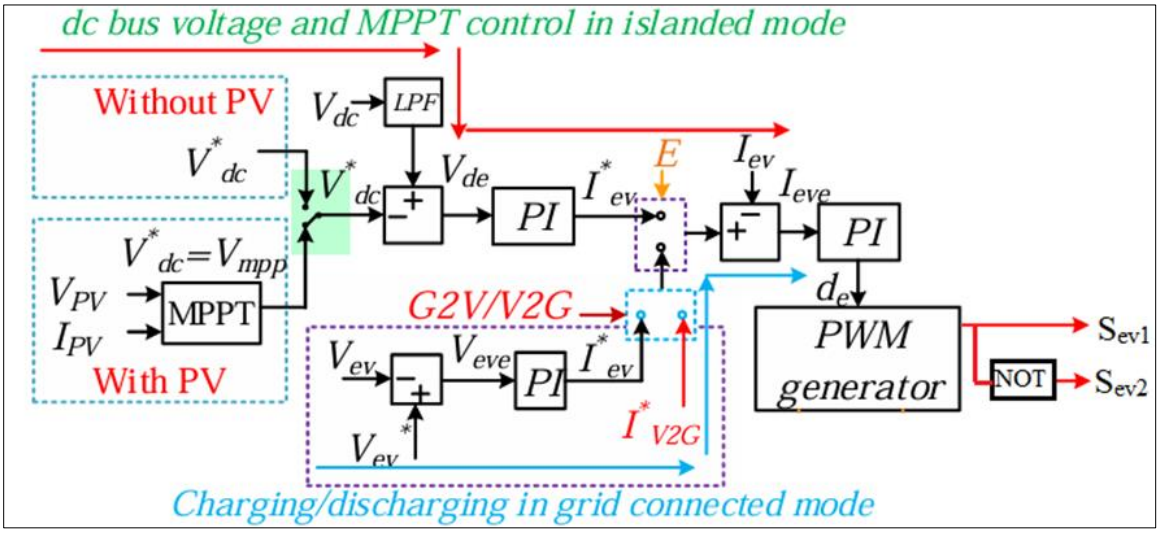

Fig. 5 BD-SEPIC control structure

The MOSFET switches S_{ev1} and S_{ev2} are operated complementarily, avoiding the short circuit of the converter. During charging mode, the BD-SEPIC converter acts as a Buck converter, which steps down the voltage on the EV battery [19]. During discharging mode, the converter acts as a Boost converter, which boosts the EV battery voltage, sharing power with the grid. As per the duty ratio (D) of these switches, the mode of operation of the converter is changed, which either charges the battery or discharges, which is determined by the below relational comparisons.

$$\left.\begin{matrix} If\ D_{S_{ev1}} > 0.5 \\ and\ \ D_{S_{ev2}} < 0.5 \end{matrix}\right\} \text{– Charging Mode (Buck Mode)}$$

$$\left.\begin{matrix} If\ D_{S_{ev1}} < 0.5 \\ and\ \ D_{S_{ev2}} > 0.5 \end{matrix}\right\} \text{– Discharging Mode (Boost Mode)}$$

With respect to these duty ratios ($D_{S_{ev1}} D_{S_{ev2}}$) the passive elements (L_1 L_2 C_1 C_2) are charged and discharged, controlling the converter operating mode. The values of these passive elements are designed by the expressions given below [20].

$$L_1 = \frac{1}{\eta f_s}\left(\frac{V_{in}^2}{P_{max}}\right)\left(\frac{V_{dc}}{V_{in}+V_{dc}}\right) \quad (10)$$

$$L_2 = \frac{V_{dc}}{2V_{in}f_s}\left(\frac{V_{in}^2}{P_{max}}\right)\left(\frac{V_{dc}}{V_{in}+V_{dc}}\right) \quad (11)$$

$$C_1 = \frac{P_i}{\kappa f_s (V_{in}+V_{dc})^2} \quad (12)$$

$$C_2 = \frac{P_{in}}{2\omega\delta V_{dc}^2} \quad (13)$$

Here, V_{in} and V_{dc} are the input and output voltage to the converter, P_{max} is the maximum power transfer, η is the permitted ripple current taken as 20%, f_s is the switching frequency, κ is the permitted ripple voltage taken as 25%, ω is the angular frequency of the grid taken as 2πf and δ output voltage ripple tolerance taken as 3% [20]. The switches S_{ev1} and S_{ev2} are controlled by EV V2G/G2V controllers as per the structure provided in Figure 5.

As per Figure 5, the EV reference current (I*ev) has either a positive or negative amplitude value. The positive value ($+I^*_{ev}$) represents the discharge of the battery, and the negative value ($-I^*_{ev}$) represents the charging of the battery in MATLAB software. This value is determined per the grid availability switched by signal (E). In grid-connected mode, two possibilities of operating modes (V2G or G2V) are defined as per the input given at the I^*_{ev}. For V2G operating mode, the EV battery needs to be discharged, and voltage is provided to the grid [6]. In this condition, the BD-SEPIC converter operates in boost mode, discharging the EV battery. The I^*_{ev} (positive value) is manually given by the user as per the grid requirement. During G2V operating mode (charging mode), the reference current is generated by the expression:

$$I^*_{ev\,(grid)} = (V^*_{ev} - V_{ev}) \left(K_p + \frac{K_i}{s}\right) \quad (14)$$

The I*ev is generated in islanding mode based on the PV panel availability. The same expression (14) is used to generate reference current. Perhaps the value V^*_{ev} is generated by the MPPT algorithm if a PV panel is available, represented as Vmpp (Voltage at the maximum power point). Without a PV panel, the value is defined according to the requirement of the DC link [6]. The final duty ratio (d_e) for controlling the BD-SEPIC converter is given as:

$$d_e = (I^*_{ev} - I_{ev}) \left(K_{pd} + \frac{K_{id}}{s}\right) \quad (15)$$

This generated de signal is compared to high frequency sawtooth or triangular waveform generating pulses to the switches S_{ev1} and the S_{ev2} receives NOT gate signal of S_{ev1}. This controls the operating mode of the BD-SEPIC converter, changing the modes of the EV battery from V2G to G2V.

4. Simulation Analysis

Modeling the circuit topologies with grid connection, PV source, and EV battery pack is performed in the MATLAB Simulink environment based on the given design and module configuration. All the blocks for the simulation modeling are considered from the 'Electrical' division of the Simulink library browser. The parameters of the blocks in the simulation are updated as per the given configuration parameters in Table 1.

Table 1. Configuration parameters

Name of the Module	Parameters
Grid	1-ph 230V_{rms} 50Hz, L_g = 1mH, C_f = 100µF, Load = 2kW
PV module	Manufacturer: 1Soltech 1STH-350-WH V_{mp} = 43V, I_{mp} = 8.13A, V_{oc} = 51.5V, I_{sc} = 9.4A, N_p = 1, N_s = 10, P_{pv} = 3.5kW Boost converter: L_b = 1mH, C_{pv} = 1000µF, R_{igbt} = 1mΩ.
EV module	Battery pack: V_{nom} = 240V, Capacity = 35Ah Conventional DC/DC converter: L_{bb} = 2.6mH, C_{bb} = 1000µF, R_{igbt} = 1mΩ, f_s = 20kHz
VSC	C_{dc} = 2200µF, $\gamma = 0.1, \sigma = 0.2$, $\delta = 1.5$, Kdc = 0.01, k =1.414, λ = 49298, f_c = 5kHz
BD-SEPIC	$L_1 = L_2$ = 2.5mH, C_1 = 80.7µF, C_2 = 1000µF, R_{mosfet} = 0.1Ω, f_s = 20kHz.

The simulation is performed under various operating conditions, including grid-connected, grid islanding, availability of PV source, no PV source, and EV module V2G/G2V modes. A comparative analysis with a conventional bidirectional DC/DC converter and BD-SEPIC converter in the EV charging module is presented in graphical representations.

The same operating conditions are maintained for both Simulink models for a simulation time of 2s. In the given simulation time, the grid is isolated at 1s, and solar insolation (Ir) is varied from 1000W/m^2 to 500W/m^2 at 0.75s, which later increased to 700W/m^2 at 1.5s. Results for different modes of EV modules are presented with graphs of each module's voltages, currents, and powers plotted concerning time.

As per the changes in the Ir value, the PV panel characteristics are presented in Figure 6. The voltage and current of the PV panel (Vpv and Ipv) drop from 240V to 150V and 12A to 8A, respectively, at 0.75s. The Vpv and Ipv values rise back to 200V and 12A at 1.5s. The PV power (Ppv) changes from 2.9kW to 1.7kW at 0.75s and rises back to 2.4kW at 1.5s as per the Ir variation. The complete power is either shared with the grid side load or with the EV battery pack for charging. As per the changes in the PV power, the EV battery operating mode changes from G2V and V2G. The characteristics of the EV battery pack for the given Ir values are presented in Figure 7.

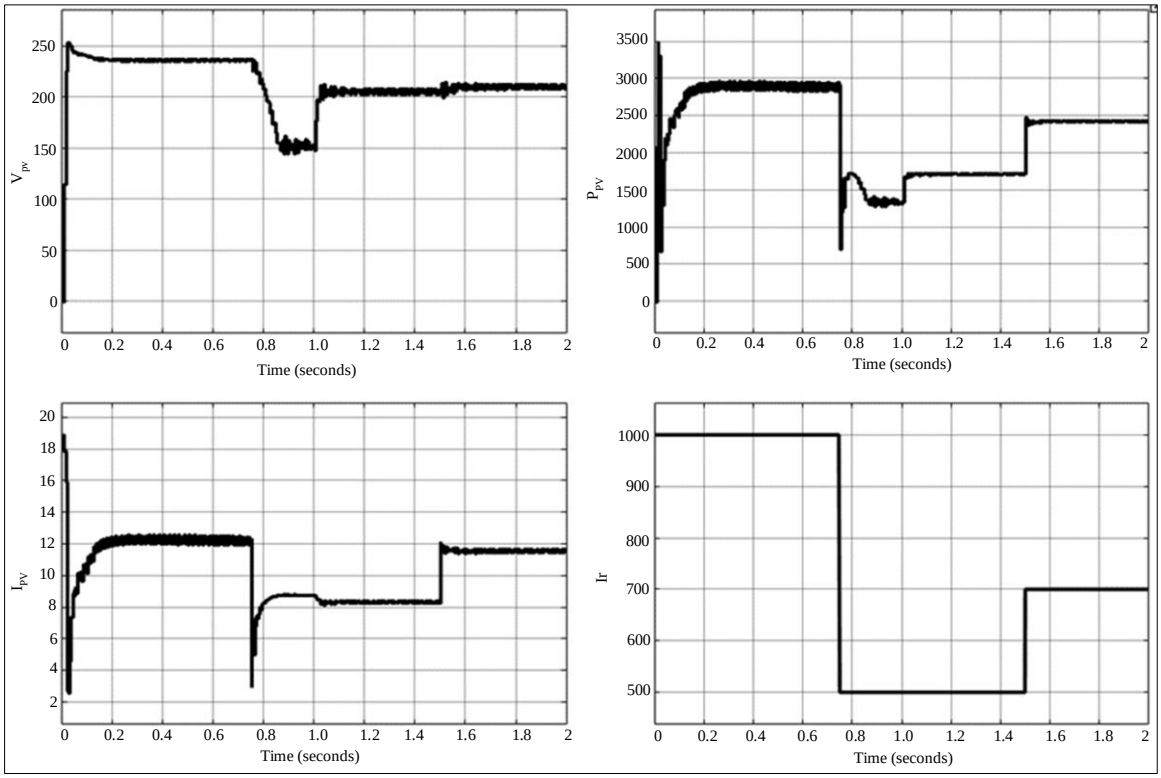

Fig. 6 PV characteristics (a) PV voltage, (b) PV current, (c) PV power, and (d) Irradiation.

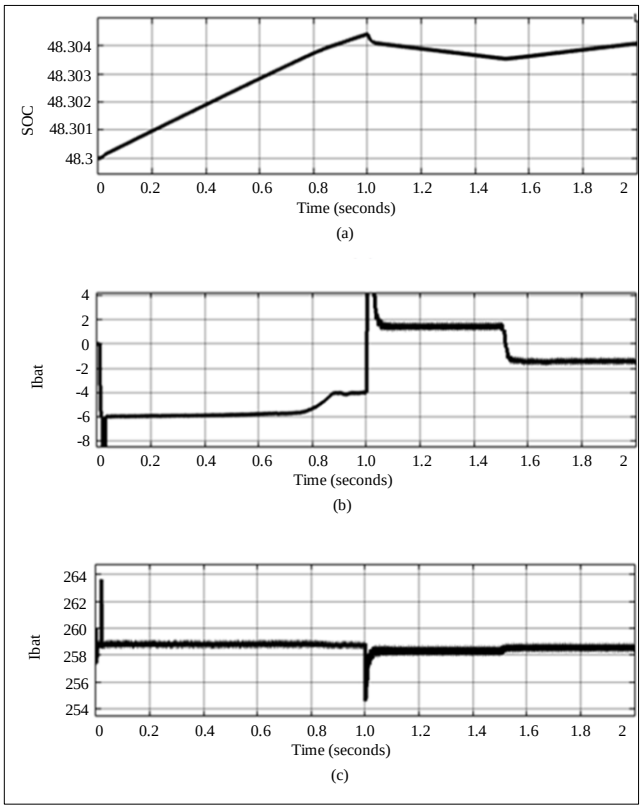

Fig. 7 EV battery characteristics (a) Battery SOC, (b) Battery current, and (c) Battery voltage.

As per Figure 7, the initial SOC is set at 48.3%, raising with a charging current of -6A until 1s, representing the G2V condition. The current direction and amplitude change from -6A to +2A at 1s, representing the V2G condition. The EV battery is discharged as the load on the AC side needs power for compensation as the grid is disconnected at 1sec. As the Ppv of 1.7kW is insufficient for the 2kW load, the remaining 0.3kW is extracted from the EV battery pack during grid isolation conditions. When the I_r value rises back to 700W/m^2 at 1.5s, the P_{pv} increases to 2.4kW, generating 0.4kW excess power after load compensation is fed to the EV battery pack charging it. The change in d_e value of the BD-SEPIC converter controller can be observed in Figure 8.

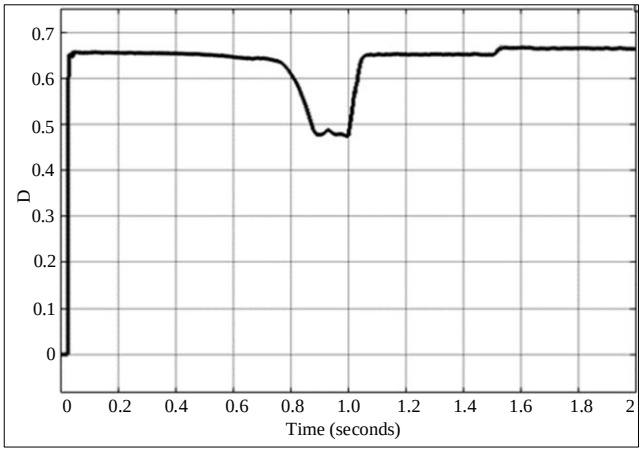

Fig. 8 Duty ratio (d_e) of the BD-SEPIC converter controller

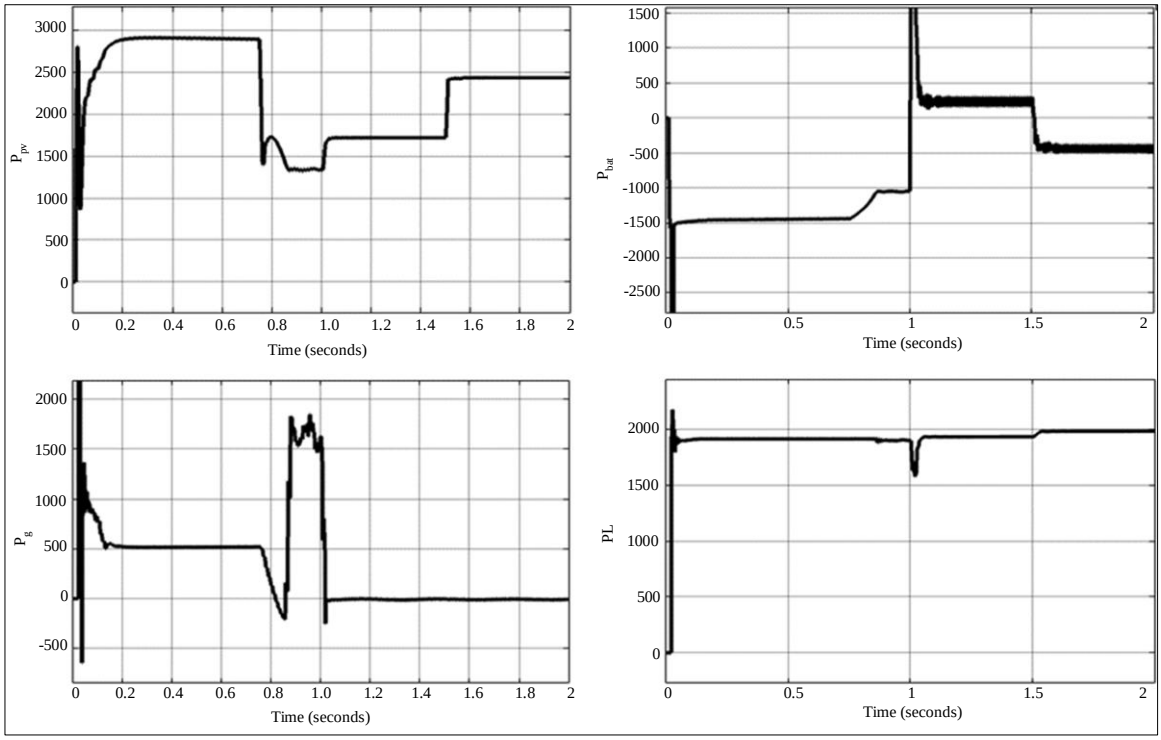

Fig. 9 Active powers of the modules (a) PV power, (b) Grid power, (c) Battery power, and (d) Load power.

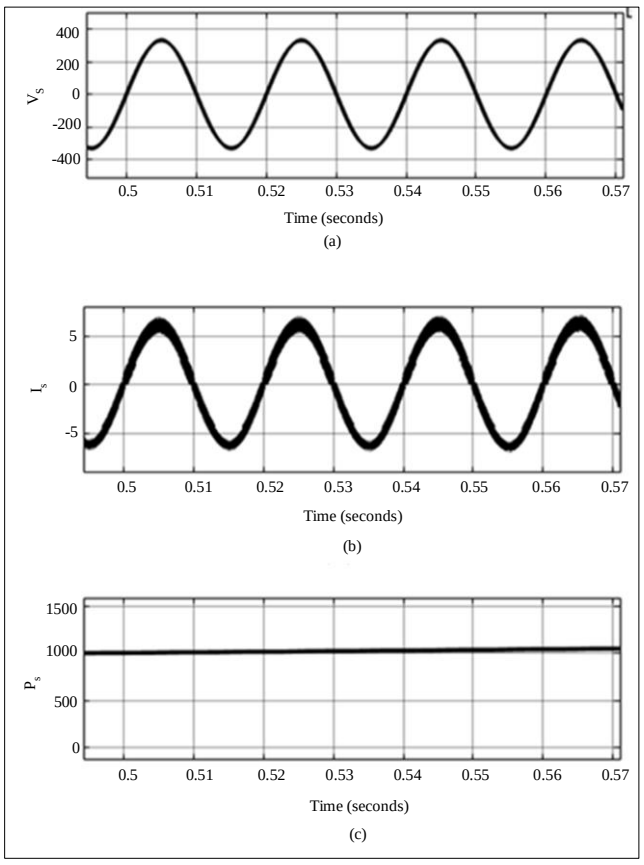

Fig. 10 VSC (a) Voltage, (b) Current, and (c) Power.

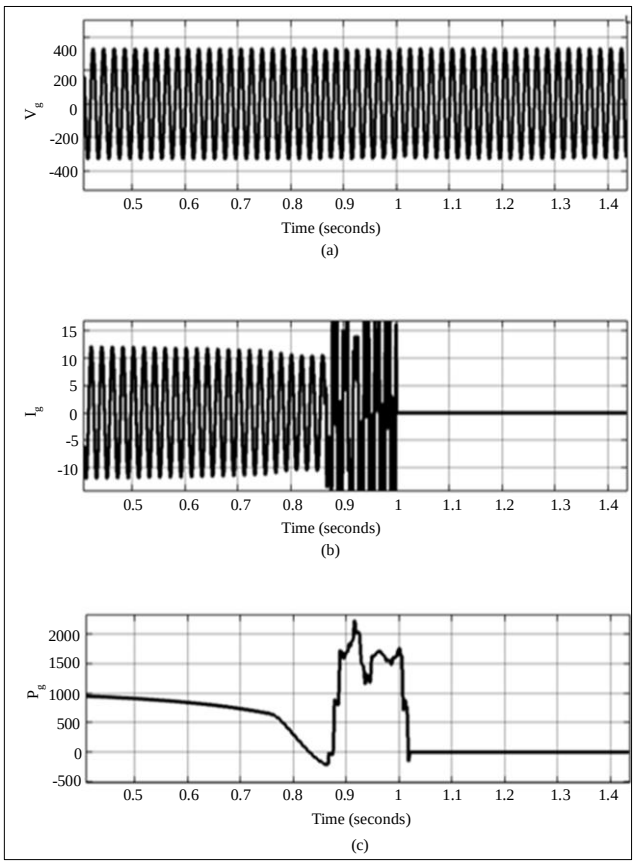

Fig. 11 Grid (a) Voltage, (b) Current, and (c) Power.

As per the given de value, the EV battery charges when de > 0.5 and discharges when de < 0.5. As per the changes in the system, the active powers of the modules in the circuit topology are presented in Figure 9. As per Figure 9, it is observed that the grid power goes to zero due to grid disconnection when the back-to-back IGBTs stop receiving the ON signal. As per the Ppv and grid availability, the EV battery module exchanges power maintaining the load power (PL) at 2kW throughout the simulation of 2s.

The VSC voltage (Vs), current (Is) and power (Ps) graphs are presented in Figure 10. The amplitude of Vs and Is are recorded to be 325V and 6A, delivering 1kW Ppv to the load. For the same grid, voltage (Vg), current (Ig) and power (Pg) are presented in Figure 11. As per Figure 11, it is observed that the Vg maintains at 325V, but the Ig drops to 0A as the grid is disconnected. The Pg shifts from 1kW to 0kW at 1s with a small transient from 0.9s to 1s when the Ir drops.

The Ppv is more stable when operated with a boost converter controlled by P&O MPPT. The Ppv comparison without and with the converter is shown in Figure 12. The Iev comparison with conventional DC/DC converter and BD-SEPIC converter is presented in Figure 13.

The amplitude of Iev is high with the BD-SEPIC converter compared to the conventional converter, as the switching losses are decreased. As per the change in Iev the battery power (Pev) is increased by 400W during charging or discharging, which can be observed in Figure 14.

The Total Harmonic Distortion (THD) of the Vs and Is signal calculated by the FFT analysis tool is presented in Figure 15. As per the analysis, both the THDs are maintained below 5% as per the IEEE 519-2022 standard in a low voltage grid system.

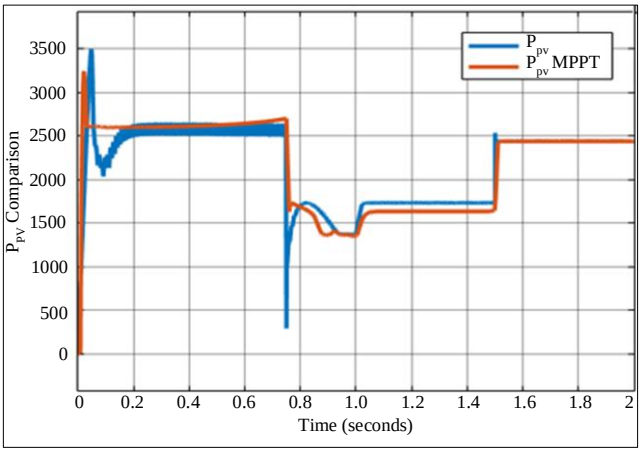

Fig. 12 PV power comparison without and with boost converter controlled by MPPT

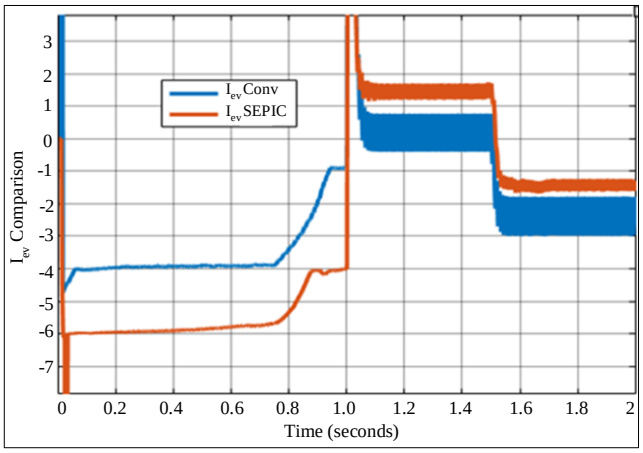

Fig. 13 EV battery current (I_{ev}) comparison between conventional DC/DC converter and BD-SEPIC converter

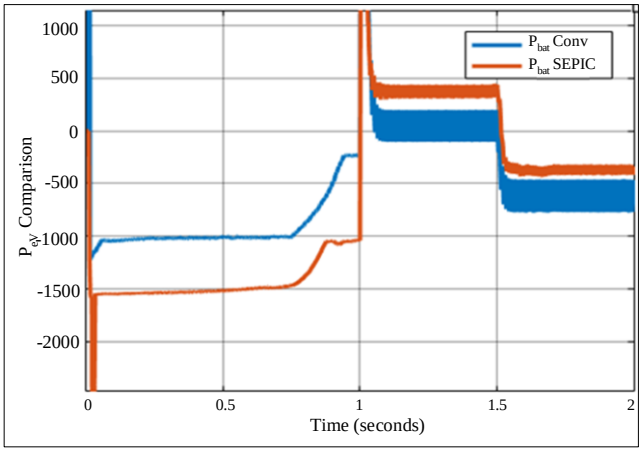

Fig. 14 EV battery power (P_{bat}) comparison between conventional DC/DC converter and BD-SEPIC converter

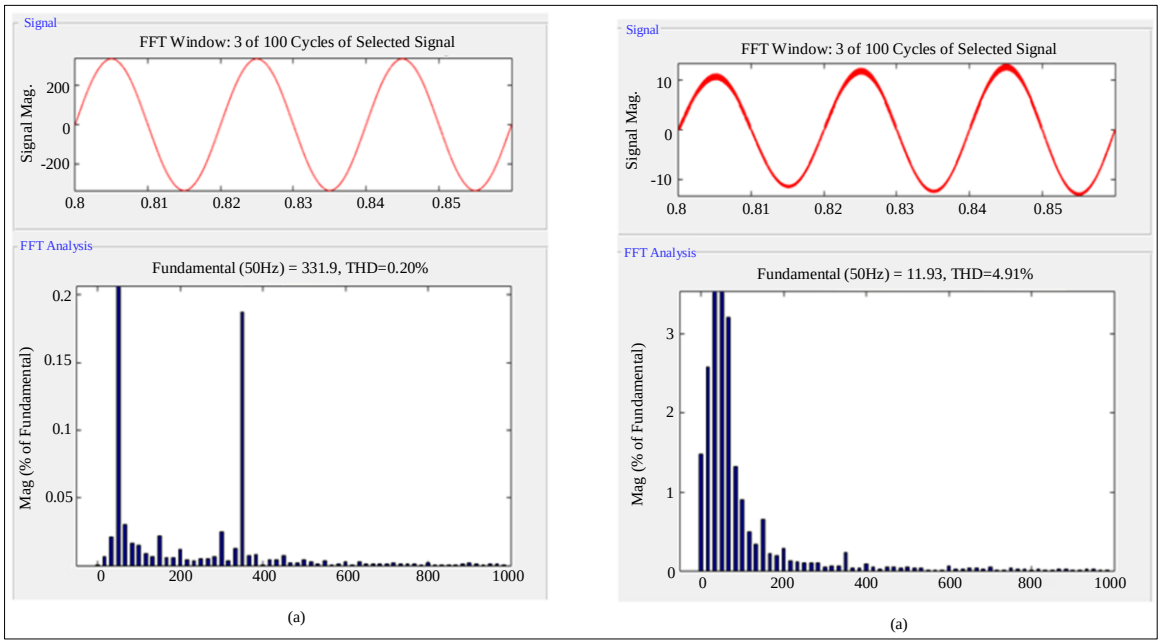

Fig. 15 THD of inverter (a) Voltage, and (b) Current.

5. Conclusion

As per the design of the proposed circuits in the system, it is determined that the multifunctional charger is more stable when operated with a BD-SEPIC converter. The power delivered and stored in the EV battery is also improved with reduced ripple content. There is a significant decrease of 25% ripple in the EV battery current compared between conventional DC/DC converter and BD-SEPIC converter. As the EV battery module generates stable power at reduced ripple current, the DC link voltage stability improves, enhancing the performance of the VSC. The VSC voltage and current have very low THDs of 0.2% and 4.91%, respectively, because of the increased stability at the DC link due to the BD-SEPIC converter operation. The load connected on the AC side is always compensated even during grid isolation and low Ppv conditions set in the simulation. The load power is compensated by the grid PV panels or EV battery, creating a robust system. The EV battery operates in V2G or G2V conditions with respect to the power generated by the PV panels and grid availability. The control structures of the VSC and BD-SEPIC converter ensure clean AC voltage and DC link stability in the system.

References

[1] Vinit Kumar et al., "PV Based Off-Grid Charging Station for Electric Vehicle," *IFAC-PapersOnLine*, vol. 52, no. 4, pp. 276-281, 2019. [CrossRef] [Google Scholar] [Publisher Link]

[2] Gamal Alkawsi et al., "Review of Renewable Energy-Based Charging Infrastructure for Electric Vehicles," *Applied Sciences*, vol. 11, no. 9, 2021. [CrossRef] [Google Scholar] [Publisher Link]

[3] Sumit Kumar, and Kiran Kumar Jaladi, "Grid Connected Electric Vehicle Charging Station Using PV Source," *2020 First IEEE International Conference on Measurement, Instrumentation, Control and Automation (ICMICA)*, Kurukshetra, India, pp. 1-4, 2020. [CrossRef] [Publisher Link]

[4] Anindya Bharatee, Pilla Sai Abhishek, and Pravat Kumar Ray, "Design of a PV-Integrated EV Charging Station with Power Management Schemes," *2023 5th International Conference on Energy, Power and Environment: Towards Flexible Green Energy Technologies (ICEPE)*, Shillong, India, pp. 1-6, 2023. [CrossRef] [Google Scholar] [Publisher Link]

[5] B. Preetha Yesheswini et al., "Solar PV Charging Station for Electric Vehicles," *2020 International Conference for Emerging Technology (INCET)*, Belgaum, India, pp. 1-7, 2020. [CrossRef] [Google Scholar] [Publisher Link]

[6] Anjeet Verma et al., "An Implementation of Solar PV Array Based Multifunctional EV Charger," *2018 IEEE Transportation Electrification Conference and Expo (ITEC)*, Long Beach, CA, USA, pp. 531-536, 2018. [CrossRef] [Google Scholar] [Publisher Link]

[7] Al Jaber Mahmud et al., "Optimal Control and Performance Enhancement of DC-DC Bidirectional SEPIC Converter," *2022 IEEE 13th Annual Ubiquitous Computing, Electronics & Mobile Communication Conference (UEMCON)*, New York, NY, USA, pp. 0437-0443, 2022. [CrossRef] [Google Scholar] [Publisher Link]

[8] Soukaina Boudoudouh, and Mohammed Maaroufi, "Renewable Energy Sources Integration and Control in Railway Microgrid," *IEEE Transactions on Industry Applications*, vol. 55, no. 2, pp. 2045-2052, 2019. [CrossRef] [Google Scholar] [Publisher Link]

[9] Osama M. Arafa et al., "Realization of Single-Phase Single-Stage Grid-Connected PV System," *Journal of Electrical Systems and Information Technology*, vol. 4, no. 1, pp. 1-9, 2017. [CrossRef] [Google Scholar] [Publisher Link]

[10] Santosh S. Raghuwanshi, and Kamlesh Gupta, "Modeling of a Single-Phase Grid-Connected Photovoltaic System Using MATLAB/Simulink," *2015 International Conference on Computer, Communication and Control (IC4)*, Indore, India, pp. 1-5, 2015. [CrossRef] [Google Scholar] [Publisher Link]

[11] Hao Yi et al., "Impedance Analysis of SOGI-FLL-Based Grid Synchronization," *IEEE Transactions on Power Electronics*, vol. 32, no. 10, pp. 7409-7413, 2017. [CrossRef] [Google Scholar] [Publisher Link]

[12] Sajad Abdali Nejad et al., "SOGI-FLL Grid Frequency Monitoring with an Error-Based Algorithm for a Better Response in Face of Voltage Sag and Swell Faults," *Electronics*, vol. 10, no. 12, 2021. [CrossRef] [Google Scholar] [Publisher Link]

[13] Nupur Saxena et al., "Implementation of a Grid-Integrated PV-Battery System for Residential and Electrical Vehicle Applications," *IEEE Transactions on Industrial Electronics*, vol. 65, no. 8, pp. 6592-6601, 2018. [CrossRef] [Google Scholar] [Publisher Link]

[14] Viet Thang Tran, Kashem M. Muttaqi, and Danny Sutanto, "A Robust Power Management Strategy with Multi-Mode Control Features for an Integrated PV and Energy Storage System to Take the Advantage of ToU Electricity Pricing," *IEEE Transactions on Industry Applications*, vol. 55, no. 2, pp. 2110-2120, 2019. [CrossRef] [Google Scholar] [Publisher Link]

[15] Hiroshi Kikusato et al., "Electric Vehicle Charge-Discharge Management for Utilization of Photovoltaic by Coordination between Home and Grid Energy Management Systems," *IEEE Transactions on Smart Grid*, vol. 10, no. 3, pp. 3186-3197, 2019. [CrossRef] [Google Scholar] [Publisher Link]

[16] Harun Turker, and Seddik Bacha, "Optimal Minimization of Plug-In Electric Vehicle Charging Cost With Vehicle-to-Home and Vehicle-to-Grid Concepts," *IEEE Transactions on Vehicular Technology*, vol. 67, no. 11, pp. 10281-10292, 2018. [CrossRef] [Google Scholar] [Publisher Link]

[17] Zhehan Yi, Wanxin Dong, and Amir H. Etemadi, "A Unified Control and Power Management Scheme for PV-Battery-Based Hybrid Microgrids for Both Grid-Connected and Islanded Modes," *IEEE Transactions on Smart Grid*, vol. 9, no. 6, pp. 5975-5985, 2018. [CrossRef] [Google Scholar] [Publisher Link]

[18] Hsiang-Yuan Lee et al., "Design and Implementation of a Bidirectional SEPIC-Zeta DC-DC Converter," *2014 IEEE International Symposium on Circuits and Systems (ISCAS)*, Melbourne, Australia, pp. 101-104, 2014. [CrossRef] [Google Scholar] [Publisher Link]

[19] P.K. Gayen, P. Roy Chowdhury, and P.K. Dhara, "An Improved Dynamic Performance of Bidirectional SEPIC-Zeta Converter Based Battery Energy Storage System Using Adaptive Sliding Mode Control Technique," *Electric Power Systems Research*, vol. 160, pp. 348-361, 2018. [CrossRef] [Google Scholar] [Publisher Link]

[20] Vashist Bist, and Bhim Singh, "Reduced Sensor Configuration of a Power Factor Correction Based Single-Ended Primary Inductance Converter Fed Brushless DC Motor Drive," *IET Power Electronics*, vol. 8, no. 9, pp. 1606-1615, 2015. [CrossRef] [Google Scholar] [Publisher Link]